



OPEN

Phase engineering of layered anode materials during ion-intercalation in Van der Waal heterostructures

Shayani Parida¹, Arthur Doble², C. Barry Carter^{3,4} & Avinash M. Dongare¹✉

Transition metal dichalcogenides (TMDs) are a class of 2D materials demonstrating promising properties, such as high capacities and cycling stabilities, making them strong candidates to replace graphitic anodes in lithium-ion batteries. However, certain TMDs, for instance, MoS₂, undergo a phase transformation from 2H to 1T during intercalation that can affect the mobility of the intercalating ions, the anode voltage, and the reversible capacity. In contrast, select TMDs, for instance, NbS₂ and VS₂, resist this type of phase transformation during Li-ion intercalation. This manuscript uses density functional theory simulations to investigate the phase transformation of TMD heterostructures during Li-, Na-, and K-ion intercalation. The simulations suggest that while stacking MoS₂ layers with NbS₂ layers is unable to limit this 2H → 1T transformation in MoS₂ during Li-ion intercalation, the interfaces effectively stabilize the 2H phase of MoS₂ during Na- and K-ion intercalation. However, stacking MoS₂ layers with VS₂ is able to suppress the 2H → 1T transformation of MoS₂ during the intercalation of Li, Na, and K-ions. The creation of TMD heterostructures by stacking MoS₂ with layers of non-transforming TMDs also renders theoretical capacities and electrical conductivities that are higher than that of bulk MoS₂.

Lithium-ion batteries (LIBs) are rechargeable energy storage devices that are rapidly replacing nickel–cadmium and nickel metal hybrid batteries^{1,2}. LIBs' main benefits over their counterparts include their high energy density, no memory effect, and low self-discharge^{3–5}. However, LIBs present their own production and performance challenges, including, but not limited to, the scarcity of Li and its expensive mining process and limited theoretical capacity of 372 mAh/g for graphitic anodes^{6,7}. Thus, current efforts seek to identify intercalating species that could substitute Li in the next generation batteries as well as discover/design anode materials beyond graphite. Potential candidates for intercalating species include other monovalent metals, such as Na^{8,9} and K^{10,11}, and multivalent metals, such as Mg^{12–15}, Ca^{12,15,16}, and Al^{12,15,17}. Similarly, potential candidates for anodes are transition metal dichalcogenides (TMDs) owing to their high capacities and large interlayer spacings for facile movement of intercalating ions^{18–20}.

Understanding the behavior of TMDs at the atomic level is crucial to predict their structural stability during charge–discharge cycles when they are used as anodes in batteries. TMDs, including MoS₂, can exhibit multiple phases depending on the coordination of the chalcogen atoms around the metal atoms, primarily the 2H (where the metal lies at the center of a trigonal prismatic coordination sphere) and 1T (where the metal lies at the center of an octahedral coordination sphere) phases. Upon intercalation of Li-ions, MoS₂ transforms from 2H to 1T phase^{21,22}. On the other hand, such a phase transformation does not occur in certain TMDs, such as NbS₂ and VS₂^{23,24}. The intercalation of metal ions in MoS₂ layers leads to a transfer of electrons from the ion to MoS₂. The excess negative charge around Mo leads to a change of the coordination state around the Mo atom, resulting in a transition from the 2H to 1T phase²⁵. On the other hand, experiments have shown that the hexagonal 2H phase of NbS₂ is stable at high Li concentrations during cell cycling^{26,27}. The 2H phase of NbS₂ is observed to be more stable than the 1T phase upon gaining electrons. Thus, electropositive ions, like Li, Na, K, etc., which donate electrons upon intercalation, do not cause phase transformation in NbS₂. On the contrary, phase transformation of NbS₂ has been proposed to be possible upon intercalation of electron-accepting impurities²³.

When metal ions intercalate into the bulk of MoS₂, in-situ TEM characterization suggests that the ion concentration is not uniform throughout the lattice. This leads to the formation of packets of lithiated regions with varying concentrations within the lattice^{28–30}. Both experimental and computational studies have suggested that

¹Department of Materials Science and Engineering, University of Connecticut, Storrs, CT, USA. ²EaglePitcher Technologies, Providence, RI, USA. ³Department of Chemical and Biomolecular Engineering, University of Connecticut, Storrs, CT, USA. ⁴Center for Integrated Nanotechnologies (CINT), Sandia National Laboratories, Albuquerque, NM, USA. ✉email: dongare@uconn.edu

the ion-intercalated regions tend to phase transform to 1T while the non-intercalated regions remain in the 2H phase^{22,31,32}. The two phases exhibit different ion mobilities, and their phase boundaries impede ion diffusion³³. Additionally, the interface between them experiences large stresses due to volumetric differences between the phases, and this can lead to mechanical failure³⁴. Thus, phase engineering, specifically the stabilization of the phases, is imperative for the improvement of battery performance.

Van der Waal (vdW) heterostructures of 2D materials promise interesting new properties which can be significantly different from the average of the properties of the individual layers^{35–37}. Unlike the creation of in-plane interfaces, the formation of interfaces in vdW heterostructures leads to clean interface structures since bond breaking or formation does not occur. vdW heterostructures have been explored for different applications^{38–40}. Zhong et al. created vdW heterostructures of ferromagnetic semiconductor CrI₃ and a TMD, WSe₂, and observed significant changes in spin and valley pseudospin in the TMD⁴¹. Xue et al. observed Moiré patterns in the heterostructures of graphene and hexagonal boron nitride⁴². In the context of batteries, Peng et al. demonstrated the use of vertical heterostructures of blue phosphorene and MS₂ (M = Nb, Ta) as flexible anode materials with capacities reaching 530 mAh/g⁴³. The vdW heterostructures of bimetallic oxychloride and reduced graphene oxides have been proposed to be suitable candidates for potassium-battery anodes⁴⁴. MoS₂ and doped graphene heterostructures have also proven to be efficient anodes for LIBs⁴⁵. There are certain avenues for the application of vdW heterostructures that are still not well understood. For instance, the synergy between stacked 2D layers can also influence the binding of intercalating ions and can potentially be exploited to regulate localized phase-transition behavior in thin films of 2D heterostructures.

This computational study investigates the phase stability of model vdW heterostructures created by stacking layered TMDs during ion intercalation. The vdW heterostructures stack layered TMDs that phase transform with those that do not phase transform to create vertical interfaces. These vertical interfaces will affect the binding of the intercalating ions and, hence, the phase stability of the layers. Density functional theory (DFT) simulations investigate the phase transformation of TMD heterostructures during Li-, Na-, and K-ion intercalation. MoS₂ is used here to model the transforming TMD layer, while NbS₂ and VS₂ represent the non-phase transforming TMD layers. The study suggests that introducing a layer of NbS₂ or VS₂ between layers of MoS₂ could potentially impede the 2H to 1T phase transformation of MoS₂ layers during Na or K intercalation. The differences in phase transformation behavior are due to the differences in charge transfer between the intercalating ion and the TMD layers. This study investigates the role of the interactions between the intercalating ions and the TMD layers on the phase stability of vdW heterostructures. In addition, the study identifies that the distribution of vertical interfaces also plays a role in impeding the phase transformation behavior during intercalation. This study identifies that introducing one non-transforming layer can impede the phase transformation behavior of only a limited number of MoS₂ layers in the vdW heterostructure. In addition, these vdW heterostructures show improved theoretical capacity and electrical conductivity.

Results and discussion

Phase transformation in bulk MoS₂, NbS₂, and VS₂ in the presence of various intercalating ions

As the first step, DFT simulations are carried out to determine the energetics of the TMD phases in the presence of Li and other intercalating ions, Na, K, Mg, Ca, and Al. Multilayered TMDs have two high symmetry sites where Li typically prefers to bind, a sixfold coordinated octahedral site (O_h) site and a fourfold coordinated tetrahedral (T_d) site. DFT calculations investigate the energetics of the three TMDs (MoS₂, NbS₂, and VS₂) in the intercalated configurations for each binding site. The energetics of the TMDs for each binding site for each intercalating ion is tabulated in Note 1 of Supplemental Information. The energies of the three TMDs in 2H and 1T phases, upon intercalation with these ions at the lowest energy sites are summarized in Table 1 and illustrated in Fig. 1. From the table, it can be concluded that intercalation of Li-, Na-, and K-ions tend to cause the transformation of MoS₂ from 2H to 1T phase, but intercalated NbS₂ and VS₂ remain in the 2H phase. Even when all the Octahedral (O_h) sites in NbS₂ or VS₂ are lithiated, the energy of 2H phase is lower than 1T phase. The results are in accordance with other studies which showed that MoS₂⁴⁶ transforms from 2H to 1T phase upon lithiation while NbS₂⁴⁶ and VS₂^{47,48} resist transformation upon lithiation. All three TMDs tend to phase transform from 2H to 1T phase in the presence of Ca and Mg, while none of them transform when Al is intercalated. This sug-

Ion	MoS ₂ (eV/formula unit)		NbS ₂ (eV/formula unit)		VS ₂ (eV/formula unit)	
	2H	1T	2H	1T	2H	1T
–			–22.61	–22.55	–20.41	–20.40
Li	–25.83	–26.06	–27.05	–26.61	–24.78	–24.50
Na	–24.95	–25.03	–26.14	–25.59	–23.96	–23.57
K	–24.30	–24.39	–25.64	–25.05	–23.25	–22.96
Mg	–24.59	–25.05	–25.45	–25.61	–23.13	–23.47
Ca	–25.98	–26.50	–26.91	–27.08	–24.56	–24.89
Al	–26.38	–26.05	–26.58	–26.40	–24.48	–24.26

Table 1. The calculated energy of 2H and 1T phases of ion intercalated MoS₂, VS₂, and NbS₂. The numbers in bold identify the lower energy phases of the TMDs in the presence of various intercalating ions.

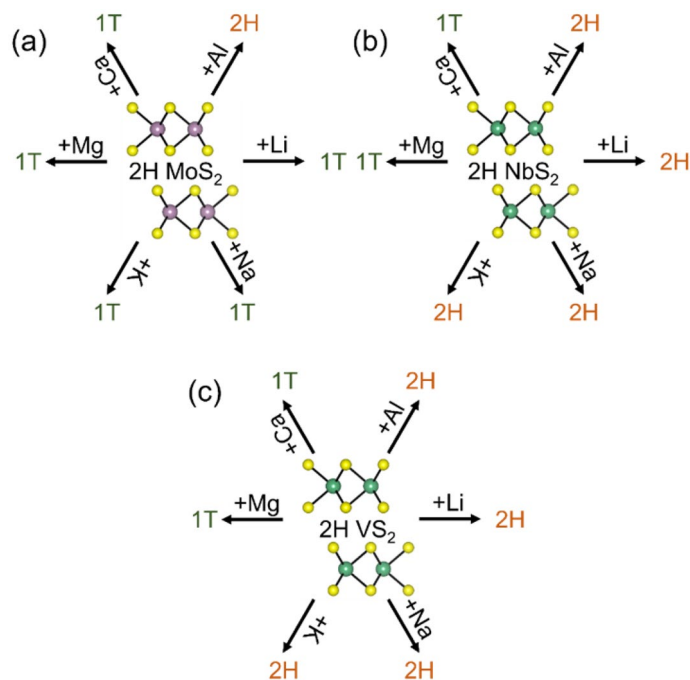


Figure 1. Schematic showing the resultant phases upon intercalation of various ions in 2H-(a) MoS₂, (b) NbS₂ and (c) VS₂.

gests that Group-I alkali metals (Li, Na, and K) lead to a phase transformation of MoS₂ but not for NbS₂ or VS₂. In addition, Group-II alkaline earth metals (Mg and Ca) lead to phase transformation of all the TMDs, and the chosen Group-III metal, Al, triggers phase transformation in none of the TMDs. Such differences in phase transformation behavior can stem from the extent of the interaction between TMDs and intercalating ions. Interesting synergistic effects can be expected during ion intercalation in heterostructures where one of the layered materials transforms while the other does not. Heterostructures of (a) NbS₂ and MoS₂ and (b) VS₂ and MoS₂ in the presence of Li, Na, and K satisfy this requirement and, therefore, are explored in this study.

Intercalation of MoS₂/NbS₂ heterostructures with Li-ions. TMD heterostructures are first created by stacking one layer of MoS₂ on top of one layer of NbS₂ to understand the effect of interfaces on the phase transformation behavior of MoS₂ and NbS₂. This creates a heterostructure of alternating MoS₂ and NbS₂ layers and is referred to as the 1-MoS₂/1-VS₂ structure, as shown in Figure S1 of the Supplementary Information. Heterostructure configurations are created to test the phase stability of the MoS₂ and the NbS₂ layers. The DFT computed energies of different phase combinations in the MoS₂/NbS₂ heterostructures are tabulated in Note 2 (Table S2A) of the Supplementary Information that suggests that the heterostructure with alternating NbS₂ and MoS₂ layers exist in the 2H phase.

DFT calculations are carried out for configurations of lithiated MoS₂/NbS₂ heterostructures with Li-ions at various high-symmetry sites to investigate the phase energetics. While multilayered TMDs only have two high-symmetry ion adsorption sites, additional high-symmetry configurations are likely in heterostructures where different TMD layers are stacked. Figure 2a–c illustrates these possible sites. While the H site has O_h symmetry, and TopMo and TopNb sites have T_d symmetry in the 2H-MoS₂/2H-NbS₂ heterostructure, as shown in Fig. 2a, the opposite is true for the 1T-MoS₂/2H-NbS₂ heterostructure. However, TopNb and TopMo represent the same site in the 1T-MoS₂/1T-NbS₂ heterostructure, as shown in Fig. 2c. Note 2 (Table S2B) of the Supplementary Information compares the energies of various lithiated phases for the possible Li binding sites. The values suggest that the energies of the lithiated heterostructure are very similar for the MoS₂ layer in the 2H and 1T phases, 1T phase slightly favored by 0.01 eV/formula unit. The previous study²² suggested that lithiation of MoS₂ layers favors a 2H → 1T phase transformation, with the 1T phase being thermodynamically more stable than the 2H phase by 0.24 eV. Thus, introducing an NbS₂ layer between two layers of MoS₂ can significantly reduce the difference in energy between the 2H and 1T phases of MoS₂.

A possible reason for the NbS₂ layer stabilizing the 2H phase in lithiated-MoS₂/NbS₂ heterostructures is the stronger binding of Li to NbS₂. The DFT calculated binding energy (BE) of Li is -2.54 eV in 2H-NbS₂ and -0.86 eV in 2H-MoS₂. This difference in Li-ion binding results in the adsorption distances between Li–NbS₂ and Li–MoS₂. The distance between the Li-ions and NbS₂ layer is calculated to be 2.45 Å and is smaller than the distance of 2.56 Å between the ions and MoS₂ layers in the heterostructure. The origins of the differences in binding can be explored by quantifying the charge transferred between 2D material and the intercalating ions. Figure 2d shows the electron localization around various atoms in the lithiated MoS₂/NbS₂ heterostructure. The contour lines show a slight difference in the localization of electron gas around the S atom attached to the Mo

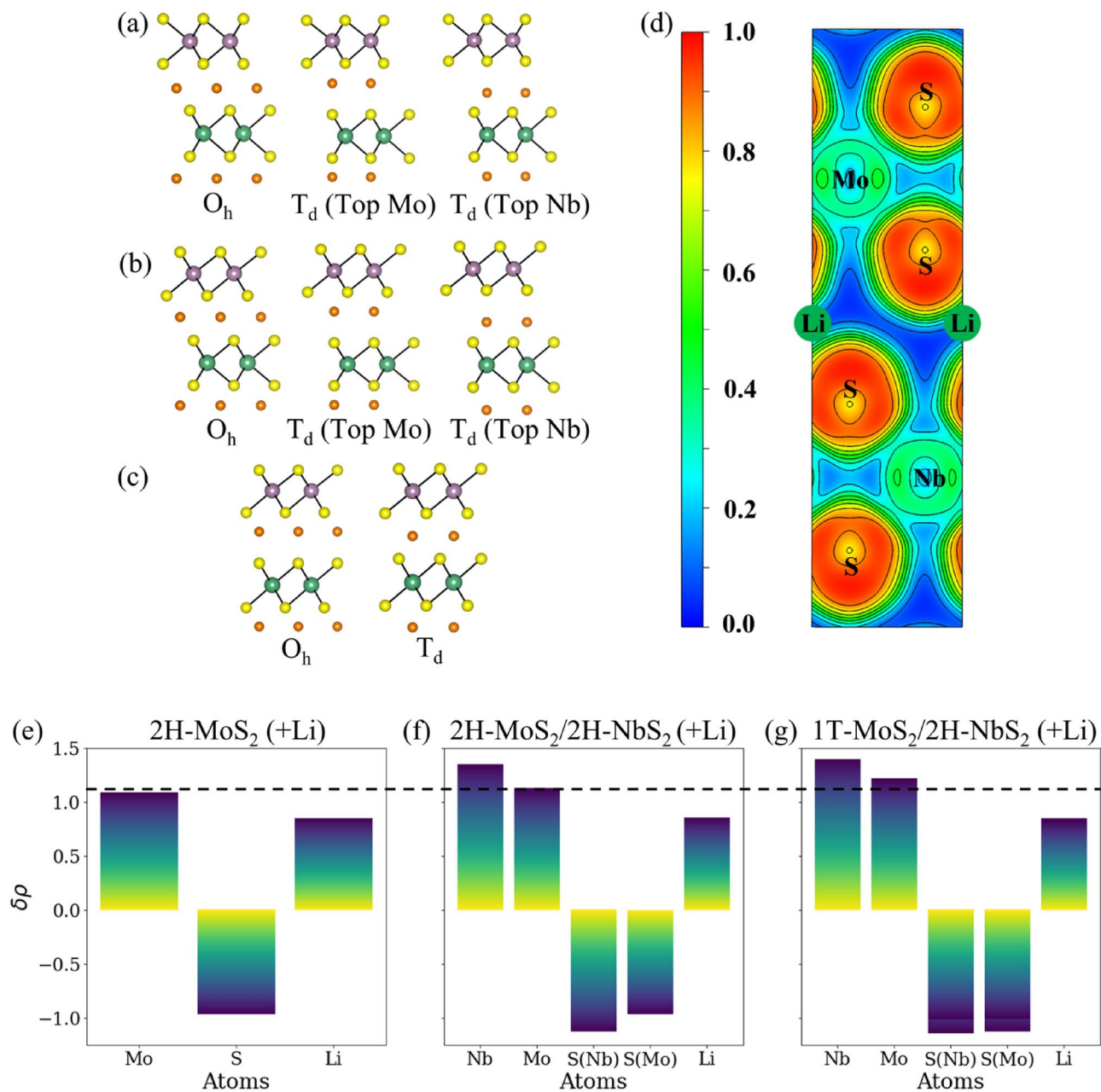


Figure 2. Different high symmetry binding sites considered for Li adsorption are shown in (a) 2H-MoS₂/2H-NbS₂, (b) 1T-MoS₂/2H-NbS₂, and (c) 1T-MoS₂/1T-NbS₂ heterostructures. Purple, green, yellow, and orange spheres denote Mo, Nb, S and Li atoms respectively. (d) Electron localization function (ELF) projected on the [100] plane of lithiated 2H-MoS₂/2H-NbS₂. A positive value implies that the atom lost electrons, while a negative value indicates that the atom has gained electrons. The dotted line, corresponding to the charge on Mo-atom in lithiated 2H-MoS₂/2H-NbS₂, is added to compare the electronic charge on Mo-atom.

atom and the S atom attached to the Nb atom. Figure 2e–g shows the charge transfer between Li-ions and multilayered 2H-MoS₂ quantified using Bader charge analysis⁴⁹. Nb is more electropositive than Mo, which would result in comparatively more electron transfer from Nb to bonded S atoms than Mo to S atoms. This difference can be clearly seen in Fig. 2f, g. Thus, S attached to Nb would have a greater electronic charge than S bonded to Mo. Hence, positively charged Li would form a stronger ionic bond with S attached to Nb than S bonded to Mo atom. The weaker interaction between Li and S attached to Mo would also result in Mo atoms not gaining enough electron charge during lithiation. Comparing the charges on the Mo atoms in multilayered MoS₂ as shown in (Fig. 2e) vs in the 2H-MoS₂/2H-NbS₂ heterostructure (Fig. 2f), Mo atoms gain more electron charges in bulk than in the heterostructure (the difference being 0.05 e⁻/Mo). The net negative charge on MoS₂ is the sum of charges on Mo and the two attached S atoms. In the same heterostructure, the net negative charge on MoS₂ is higher when it exists in the 1T (Fig. 2g) phase than in the 2H phase (Fig. 2f). The barrier for phase transformation of MoS₂ in the heterostructure in the presence of Li is calculated to be 0.85 eV, which is lower than the transition

barrier of 0.95 eV in multilayered MoS₂. So, kinetically, phase transformation of the lithiated heterostructure is also slightly more favorable than a multilayered MoS₂ system. The Bader charges on partially phase-transformed MoS₂ at the saddle point in bulk MoS₂ and the heterostructure are $-0.88 e^-$ and $-0.82 e^-$ respectively. This is again consistent with the fact that the presence of NbS₂ depletes the net negative charge on MoS₂ during Li intercalation.

Intercalation of MoS₂/NbS₂ heterostructures with Na- and K-ions. DFT calculations are also carried out for various configurations of MoS₂/NbS₂ heterostructures intercalated with Na- and K-ions at different high-symmetry sites to investigate the phase energetics. Note 2 (Table S2B) of the Supplemental Information compares the energies of various phases of the MoS₂ and NbS₂ layers in the intercalated heterostructure for the possible Na-ion and K-ion binding sites. The lowest energy phases of the intercalated heterostructures and the corresponding energies are tabulated in Table 2 for the Na-ion intercalation and K-ion intercalation in addition to that observed for Li-ion intercalation. It can be seen that the intercalated 2H-MoS₂/2H-NbS₂ heterostructure has minimum energy, wherein the H site (with O_h symmetry) is the energetically preferred binding site. Thus, Na-ion or K-ion intercalation allows the 2H phase of MoS₂ to be stable.

The top view of the intercalated heterostructure is shown in Fig. 3a. Bader analysis is used to analyze the electron transfer in the Na-ion and K-ion intercalated heterostructure, as shown in Fig. 3b,c. It can be concluded

Ion	2H-MoS ₂ /2H-NbS ₂ (eV/formula unit)	1T-MoS ₂ /2H-NbS ₂ (eV/formula unit)	1T-MoS ₂ /1T-NbS ₂ (eV/formula unit)
Li	-52.75	-52.76	-52.64
Na	-50.96	-50.66	-50.56
K	-49.93	-49.49	-49.43

Table 2. Energy of different phases of lithiated 1-MoS₂/1-NbS₂ heterostructure (with alternating layers of MoS₂ and NbS₂) after Li, Na and K intercalation. The numbers in bold identify the lower energy phases of the TMDs in the presence of various intercalating ions.

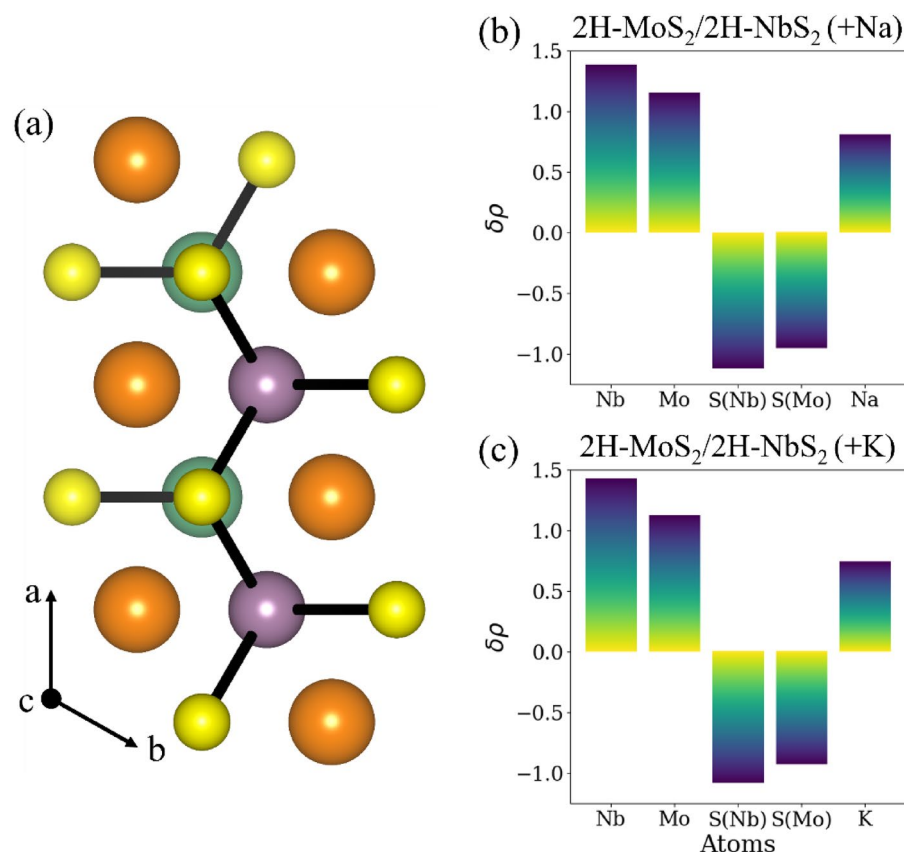


Figure 3. (a) Top view of 2H-MoS₂/2H-NbS₂ heterostructures (alternating layers of NbS₂ and MoS₂) with ions at the lowest energy binding site (O_h/H site). Charges transferred from different atoms in (b) Na-ion intercalated and (c) K-ion intercalated heterostructures are computed using Bader analysis. A positive value implies that the atom lost electrons, while a negative value indicates that the atom has gained electrons.

that S atoms attached to Nb gain more negative charges than the S atoms attached to the Mo atoms. This difference in charge transfer pulls the positively charged ions toward the NbS₂ layer. For Na-ion intercalation, the distance between the Na-ions and NbS₂ layer is calculated to be 2.73 Å and is smaller than the distance of 2.81 Å between the Na-ions and MoS₂ layers in the heterostructure. For K-ion intercalation, the distance between the K-ions and NbS₂ layer is calculated to be 3.04 Å and is smaller than the distance of 3.06 Å between the K-ions and MoS₂ layers in the heterostructure. This would again result in lesser interaction between intercalating ions and MoS₂ layers and a lesser tendency for MoS₂ to phase transform.

Thus, the key difference that explains the phase transformation of MoS₂ in the heterostructure observed during Li-ion intercalation and not during Na-ion or K-ion intercalation lies in the net negative charge on MoS₂ upon ion intercalation. The net negative charge on MoS₂ is -0.76 e⁻ for Na-ion intercalation and -0.73 e⁻ upon K-ion intercalation and is lower than the net negative charge of 0.80 e⁻ for Li intercalation. A lower net negative charge on MoS₂ impedes its phase transformation during Na-ion, and K-ion intercalation, as observed for Li-ion intercalation. The calculated barriers for phase transformation of a MoS₂ layer in the heterostructures are 0.9 eV and 0.86 eV during Na-ion and K-ion intercalation, respectively. The presence of an interface increases these transformation barriers to 1.05 eV and 0.79 eV during Na-ion and K-ion intercalation, respectively. In the heterostructure, the charges on MoS₂ at the saddle point during Na and K intercalation are -0.79 e⁻ and -0.72 e⁻.

Thus, NbS₂ exhibits stronger binding with Li-, Na-, and K-ions than MoS₂, which weakens the interaction between ions and MoS₂ during intercalation. However, it is unclear if the introduction of an NbS₂ impedes phase transformation in only the neighboring MoS₂ layers or if it can also influence the transformation behavior of non-adjacent MoS₂ layers. The study, therefore, explores the capability of each NbS₂ layer to limit to impede the phase transformation of non-adjacent MoS₂ layers in multilayered heterostructures.

Intercalation of MoS₂/NbS₂ multilayered heterostructures with more than one MoS₂ layer between two NbS₂ layers.

It is unclear if this ability to impede the Na-ion and K-ion intercalation-induced phase transformation in the MoS₂ layer by stacking a layer of NbS₂ depends on the number of the MoS₂ layers (thickness of the MoS₂ film). It remains to be verified if the NbS₂ layer impedes the phase transformation only in the adjacent MoS₂ layers or even in layers that are farther away. Hence, multilayered heterostructures are created with a repeating unit of three MoS₂ layers and one NbS₂ layer, a structure referred to as 3-MoS₂/1-NbS₂, as shown in Fig. 4a. The phase transformation in this multilayered system can occur in several different ways during ion intercalation. Hence three unique configurations of this 3-MoS₂/1-NbS₂ heterostructure are created as shown in Fig. 4a: 0L: None of the MoS₂ layers transform to the 1T phase; 1L: Only one MoS₂ layer in the middle is transformed to the 1T phase; 3L: All the three MoS₂ layers are transformed to the 1T phase. The 1L and 3L structures represent the formation of a hybrid 2H/1T phase, as depicted in Fig. 4a. The binding sites for Na- and K-ions during intercalation are investigated using high-symmetry sites to determine minimum energy configurations as tabulated in Note 3 (Table S3) of the Supplemental Information. A comparison of the energies of the Na-ion and K-ion intercalated 3-MoS₂/1-NbS₂ structures suggests that the lowest energy configuration is the one where MoS₂ layers do not phase transform and retain their 2H phase. 2H-MoS₂ is retained even when MoS₂ layers are not adjacent to NbS₂ layers. Thus, in battery anodes, the introduction of NbS₂ can provide a way to inhibit phase transformation in MoS₂ during Na-ion and K-ion intercalation. The Bader plots of the 3-MoS₂/1-NbS₂ heterostructures with three layers of MoS₂ between two layers on NbS₂, as shown in Fig. 4b, c, indicate that Na-ions and K-ions intercalated at the interface of MoS₂ and NbS₂ layers (marked with *) lose more charge than ions intercalated between two layers of MoS₂. The difference is more significant during the intercalation of Na-ions than K-ions. The net charge on MoS₂ layers is slightly more than charges on MoS₂ in the heterostructure with alternating layers of MoS₂ and NbS₂ (difference is 0.02 eV for Na-ion while for K-ions, the charges are same in the two structures), and hence, even in these structures, phase transformation is not preferred.

DFT calculations are further carried out to investigate the phase stability in multilayered heterostructures created with a repeating unit of five MoS₂ layers and one NbS₂ layer, a structure referred to as 5-MoS₂/1-NbS₂, as shown in Fig. 5a. The phase transformation in this multilayered system can occur in several different ways during ion intercalation. Hence four unique configurations of this 5-MoS₂/1-NbS₂ heterostructure are created as shown in Fig. 5a: 0L: None of the MoS₂ layers transform to the 1T phase; 1L: Only one MoS₂ layer in the middle is transformed to the 1T phase; 3L: The three MoS₂ layers in the middle are transformed to the 1T phase; 5L: The five MoS₂ layers in the middle are transformed to the 1T phase. The 1L, 3L, and 5L structures represent the formation of a hybrid 2H/1T phase. Bader charges are calculated for Na-ion and K-ion intercalated 5-MoS₂/1-NbS₂ heterostructures and these are represented in Fig. 5b, c. The total negative charge on MoS₂ is same as that seen in Na-ion and K-ion intercalated 3-MoS₂/1-NbS₂ heterostructures. The binding sites for Na- and K-ions during intercalation are investigated using high-symmetry sites to determine minimum energy configurations as tabulated in Note 4 (Table S4) of the Supplemental Information. A comparison of the energies of the Na-ion and K-ion intercalated 5-MoS₂/1-NbS₂ structures suggests that the lowest energy configuration is the one where MoS₂ layers do not phase transform and retain their 2H phase. Thus, 2H-MoS₂ is retained even when MoS₂ layers are not adjacent to NbS₂ layers.

DFT simulations are carried out for larger heterostructures by further increasing the number of MoS₂ layers to seven in the repeating unit with one NbS₂ layer, a structure referred to as 7-MoS₂/1-NbS₂. A comparison of the energies of the Na-ion and K-ion intercalated 7-MoS₂/1-NbS₂ structures suggests that the lowest energy configuration is the one where the middle MoS₂ layer (1L) phase transforms to the 1T phase. Thus, a limit is observed in the capability of one NbS₂ layer to impede the phase transformation behavior of neighboring MoS₂ layers during the intercalation of Na-ions than K-ions.

The results suggest that MoS₂/NbS₂ heterostructures where every MoS₂ layer has one NbS₂ layer as at least the third nearest-neighboring layer are an effective design for layered anodes to retain the phase stability during the

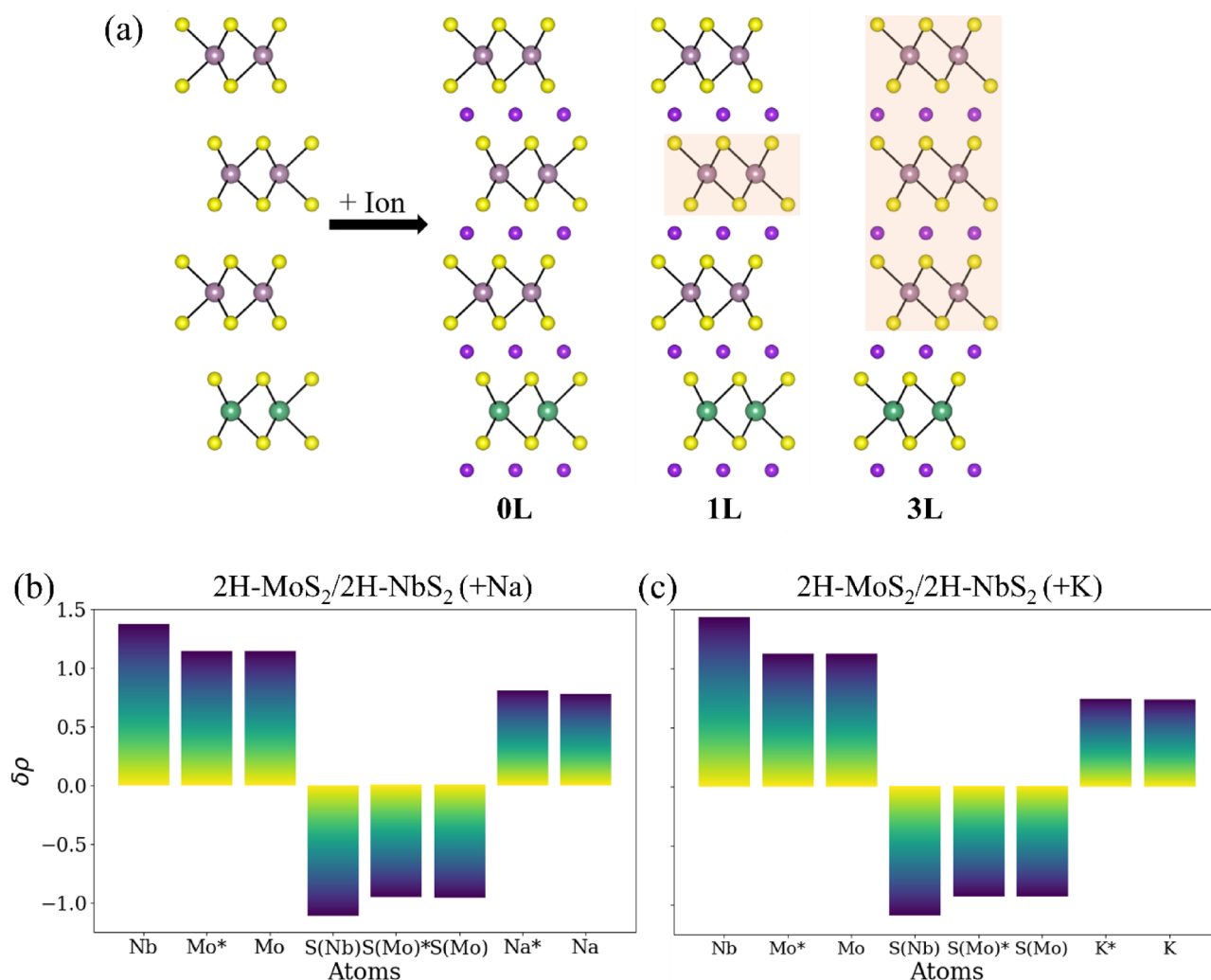


Figure 4. (a) (left) Schematic representation of the 3-MoS₂/1-NbS₂ heterostructures showing a repeating unit of three MoS₂ layers and one NbS₂ layer. Light purple, green, yellow, and darker purple spheres represent Mo, Nb, S, and intercalating ions- Na or K, respectively. 1T-MoS₂ is highlighted in orange. Charges transferred from different atoms in (b) Na-ion intercalated and (c) K-ion intercalated lowest energy structure 0L: 2H-NbS₂/2H-MoS₂ computed using Bader analysis. A positive value implies that the atom lost electrons, while a negative value indicates that the atom gained electrons. S(Mo) identifies S atoms bonded to Mo, while S(Nb) refers to S atoms bonded to Nb atoms. Asterisks (*) are marked to identify Mo and S(Mo) atoms neighboring NbS₂ layers and Na- or K-ions intercalating the interface between NbS₂ and MoS₂.

intercalation of Na-ions than K-ions. The stability of the phases is attributed to the reduction in the net negative charge on the MoS₂ layers due to the presence of the NbS₂ layer during ion intercalation. This difference in charge transfer affects the bond distances between the intercalating ions and NbS₂ layer and that between the intercalating ions and MoS₂ layers in the heterostructure as tabulated in Note 5 (Table S5) of the Supplemental Information for the various multilayered heterostructures studied here. This study, therefore, demonstrates the capability of stacking non-transforming TMD layers as an approach to impede the phase transformation of non-adjacent transforming TMD layers in multilayered heterostructures. While this is demonstrated by using NbS₂ as the non-transforming TMD layers, it is not clear if this strategy will work for other non-transforming TMD layers.

Intercalation of MoS₂/VS₂ multilayered heterostructures. DFT simulations are therefore carried out to investigate the phase stability behavior in multilayered heterostructures formed by stacking MoS₂ layers with VS₂ layers that do not transform during Li-ion, Na-ion, and K-ion intercalation. MoS₂/VS₂ heterostructures are first created by stacking one layer of MoS₂ on top of one layer of VS₂ to understand the effect of interfaces on the phase transformation behavior of MoS₂ and VS₂. This creates a monolayer heterostructure of alternating MoS₂ and VS₂ layers and also referred to as the 1-MoS₂/1-VS₂ structure. Note 6 (Table S6A) of the Supplemental Information compares the energies of various phases of the MoS₂ and VS₂ layers in the intercalated monolayer heterostructure for the possible Na-ion and K-ion binding sites. The total energies of the different phases are compared after Li-ion, Na-ion, and K-ion intercalation, as summarized in Table 3. A comparison of the energies

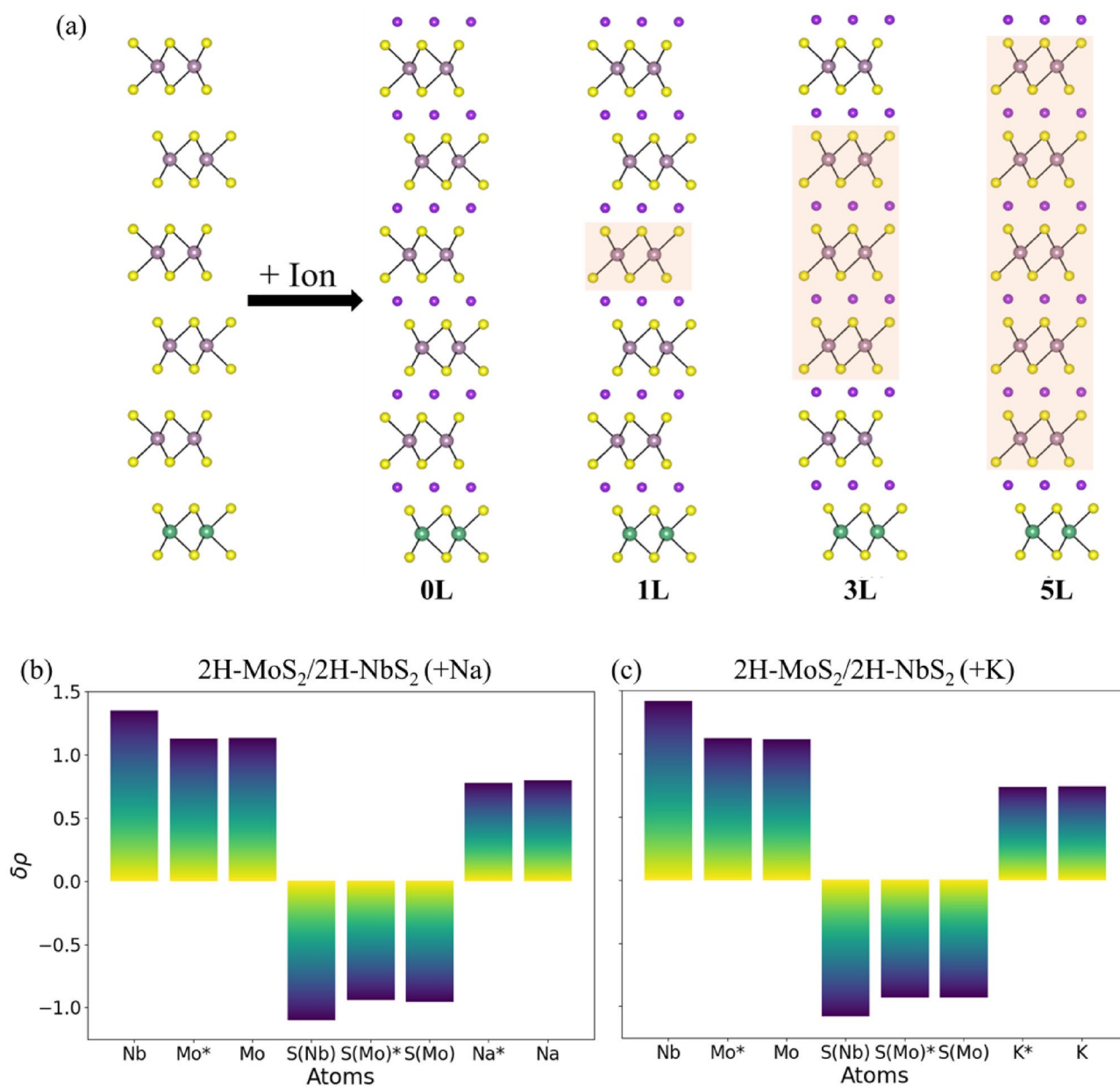


Figure 5. (a) (left) Schematic representation of the 5-MoS₂/1-NbS₂ heterostructures showing a repeating unit of five MoS₂ layers and one NbS₂ layer. Light purple, green, yellow, and darker purple spheres represent Mo, Nb, S, and intercalating ions- Na or K, respectively. 1T-MoS₂ is highlighted in orange. Charges transferred from different atoms in (b) Na-ion intercalated and (c) K-ion intercalated lowest energy structure 0L: 2H-NbS₂/2H-MoS₂ computed using Bader analysis. A positive value implies that the atom lost electrons, while a negative value indicates that the atom gained electrons. S(Mo) identifies S atoms bonded to Mo, while S(Nb) refers to S atoms bonded to Nb atoms. Asterisks (*) are marked to identify Mo and S(Mo) atoms neighboring NbS₂ layers and Na- or K-ions intercalating the interface between NbS₂ and MoS₂.

Ion	2H-MoS ₂ /2H-VS ₂ (eV/formula unit)	1T-MoS ₂ /2H-VS ₂ (eV/formula unit)	1T-MoS ₂ /1T-VS ₂ (eV/formula unit)
Li	-50.03	-49.96	-50.00
Na	-48.39	-48.05	-48.10
K	-47.05	-46.68	-46.84

Table 3. Energy of different phases of lithiated 1-MoS₂/1-VS₂ heterostructure (with alternating layers of MoS₂ and VS₂) after Li, Na and K intercalation. The numbers in bold identify the lower energy phases of the TMDs in the presence of various intercalating ions.

of the Li-ion intercalated (1-MoS₂/1-NbS₂) heterostructures suggests that the lowest energy configuration is the one where the MoS₂ layer does not phase transform and retains the 2H phase for all intercalating ions. This is different from the phase stability of the monolayer MoS₂/NbS₂ heterostructures, wherein a phase transformation was observed for Li-ion intercalation. This difference in behavior between NbS₂ and VS₂ can be related to their electronic structure and explained based on charge analysis, as shown in Fig. 6a. The net negative charge on MoS₂ in MoS₂/VS₂ heterostructures is lower than the charge on MoS₂ in MoS₂/NbS₂ heterostructures by 0.02 e⁻. This difference can result in impeding the phase transition behavior of the MoS₂ layer during Li-ion intercalation of 1-MoS₂/1-VS₂ heterostructure. Na-ion and K-ion intercalation renders even lower negative charges accumulate on the MoS₂ layer, as shown in Fig. 6b, c. As a result, no phase transformation is observed during Na-ion and K-ion intercalation. Thus, VS₂ layers are also able to impede the phase transformation of MoS₂ layers induced by the intercalation of Li-, Na-, or K-ions.

Similarly, multilayered heterostructures are created with a repeating unit of three MoS₂ layers and one VS₂ layer (a structure referred to as 3-MoS₂/1-VS₂). Similar to the MoS₂/NbS₂ heterostructures, the phase transformation in this multilayered system can occur in several different ways during ion intercalation. Hence three unique configurations of this 3-MoS₂/1-NbS₂ heterostructure are created: 0L, 1L, and 3L. The binding sites for Li-, Na-, and K-ions during intercalation are investigated using high-symmetry sites to determine minimum energy configurations as tabulated in Note 6 (Table S6B) of the Supplemental Information. A comparison of the energies of the Na-ion and K-ion intercalated 3-MoS₂/1-VS₂ structures suggests that the lowest energy configuration is the one where MoS₂ layers do not phase transform and retain their 2H phase. However, a comparison of the energetics of the intercalated 3-MoS₂/1-VS₂ structures during Li-ion intercalation suggests that the lowest energy configuration is the one where the middle MoS₂ layer (1L) phase transforms to the 1T phase. The phase transformation barriers of MoS₂ in Li and Na intercalated heterostructures are 0.9 eV and 0.94 eV, respectively, which is lower than the barriers in bulk MoS₂. The observed transformation barrier during K intercalation is 0.78 eV in the MoS₂/VS₂ heterostructures, which is similar to that seen in the bulk phase.

Thus, 2H-MoS₂ is retained even when MoS₂ layers are not adjacent to VS₂ layers for Na-ion and K-ion intercalation and when the MoS₂ layer is adjacent to the VS₂ layer during Li-ion intercalation. The ability to impede the phase transformation behavior of MoS₂ layers is dependent on the net negative charge rendered on the MoS₂ layer during ion intercalation.

Role of charge transfer on phase transformation of multilayered heterostructures. Throughout this paper, the net charge on MoS₂ is linked to relative energies of the 2H and 1T phases upon ion intercalation. The net charge on the MoS₂ layers in intercalated MoS₂/NbS₂ and MoS₂/VS₂ heterostructures is lower than in the intercalated bulk MoS₂, as shown graphically in Fig. 7a,b, respectively. As the number of MoS₂ layers in between the layers of NbS₂ or VS₂ increases, the average charge on the MoS₂ layers also increases. A slight anomaly is seen in the case of K-ion intercalation in MoS₂/NbS₂ heterostructures. Upon K-ion intercalation, the net charge on MoS₂ computed in two of the heterostructures is slightly higher than the charge on MoS₂ when present in bulk form. This anomaly is most likely due to the precision of the charge calculations since the computed charge values are so close (<0.01 e⁻). The charge on the MoS₂ within a given heterostructure is also dependent on how far it is from the NbS₂ or VS₂ layers; the MoS₂ layer closest to the NbS₂ or VS₂ layer has the lowest net charge amongst all the layers in the heterostructure. For instance, upon Li-ion intercalation of the MoS₂/VS₂ heterostructure where there are three MoS₂ layers between two layers of VS₂ (similar to Fig. 4a), the MoS₂ layers adjacent to VS₂ layers have a net charge of -0.82 e⁻ while the non-adjacent ones have a net charge of -0.84 e⁻. As discussed in previous sections, the 1T phase is more stable than the 2H phase of MoS₂ as the charge on the MoS₂ increases. This hypothesis also holds true in this MoS₂/VS₂ microstructure since the most energetically stable configuration is Fig. 4a-1L, where the MoS₂ layers adjacent to the VS₂ layers remain in 2H phase while only the non-adjacent layer transforms to 1T phase.

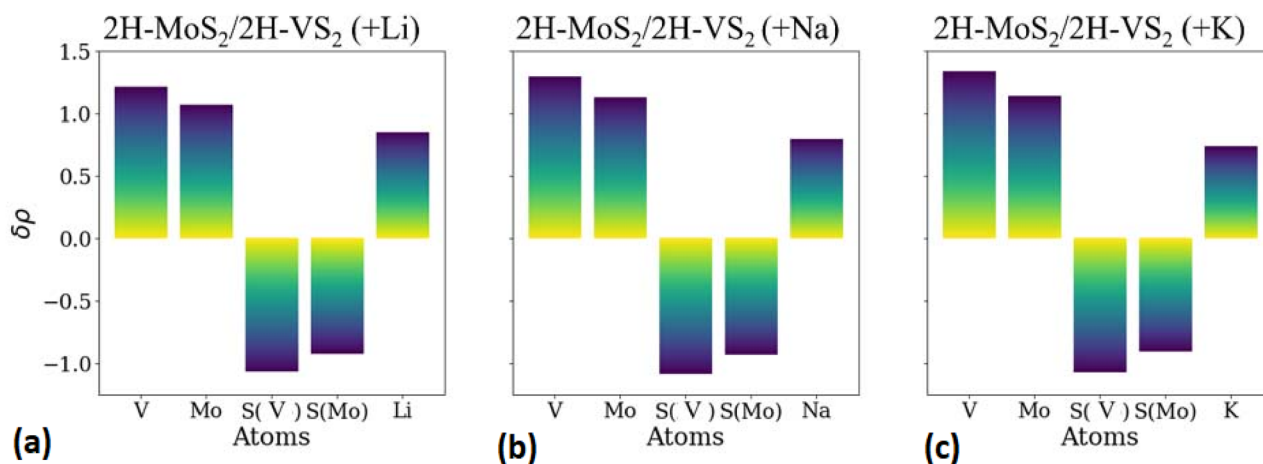


Figure 6. Charges transferred from different atoms in (a) Li-ion, (b) Na-ion and (c) K-ion intercalated 2H-MoS₂/2H-VS₂ heterostructures (alternating layers of VS₂ and MoS₂) computed using Bader analysis.

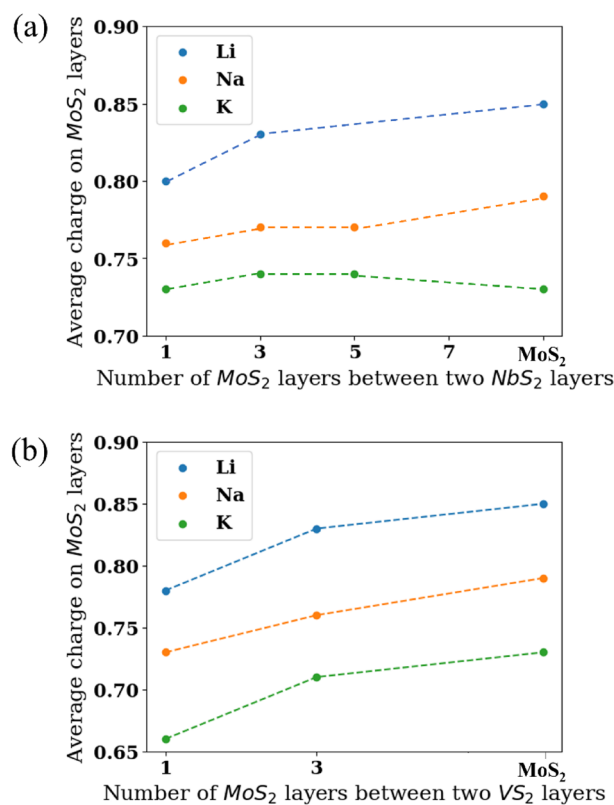


Figure 7. The average negative charge on MoS_2 layers, upon intercalation with Li-, Na-, and K-ions, as a function of the number of MoS_2 layers in between two (a) NbS_2 layers and (b) VS_2 layers. The charge on MoS_2 increases as the number of MoS_2 layers in between two NbS_2 (or VS_2) layers increases.

Capacities and Electrical band gaps of the heterostructures. An important criterion to consider while building such heterostructures is the theoretical capacities as well as the electronic conductivities for the various configurations discussed above. The calculated capacities (Note 7 of Supplemental Information⁵⁰) of 2H- MoS_2 and the monolayer $\text{MoS}_2/\text{NbS}_2$ and MoS_2/VS_2 heterostructures are summarized in Table 4. The predicted capacity for 2H- MoS_2 calculated in this study is slightly lower than the reported value of 167 mAh/g, considering a similar anode reaction^{51,52}. The difference stems from the fact that previous studies assumed that Li gives up its valance electron completely ($n = 1$), but the Bader analysis performed in this study shows that Li-, Na-, or K-ions give up partial charges during ion intercalation. Table 4 suggests that $\text{MoS}_2/\text{NbS}_2$ heterostructures show a small improvement in theoretical capacities over bulk MoS_2 . MoS_2/VS_2 heterostructures show much higher capacities giving a > 15% increase of predicted capacities over bulk MoS_2 . A significant improvement of theoretical capacities is expected since the charge transfers from the intercalating ions to the layered materials are similar in bulk MoS_2 and the heterostructures, but the molecular mass of V is much lower than Nb, which is

Intercalating ion	Layered material	Predicted capacity (mAh/g)
Li	2H- MoS_2	141.8
	2H- $\text{MoS}_2/2\text{H-NbS}_2$ (alternating layers)	144.1
	2H- $\text{MoS}_2/2\text{H-VS}_2$ (alternating layers)	165.5
Na	2H- MoS_2	131.6
	2H- $\text{MoS}_2/2\text{H-NbS}_2$ (alternating layers)	136.2
	2H- $\text{MoS}_2/2\text{H-VS}_2$ (alternating layers)	155.0
K	2H- MoS_2	121.6
	2H- $\text{MoS}_2/2\text{H-NbS}_2$ (alternating layers)	124.9
	2H- $\text{MoS}_2/2\text{H-VS}_2$ (alternating layers)	142.2

Table 4. Predicted theoretical capacities of 2H- MoS_2 and heterostructures with alternating layers of MoS_2 and NbS_2 and MoS_2 and VS_2 during Li, Na and K intercalation.

in turn lower than Mo. The reduction of the weight of the MoS₂-based anode materials due to the introduction of NbS₂ or VS₂ layers can be expected to improve their gravimetric capacities.

The density of states of bulk MoS₂ and the monolayer MoS₂/NbS₂ and the MoS₂/VS₂ heterostructures is plotted in Fig. 8. The 2H-MoS₂ phase is a semiconductor with a wide bandgap close to 0.9 eV for the bulk phase⁵³ and hence demonstrates poor electronic conductivities owing to its wide bandgap and can lead to rapid capacity degradation⁵⁴. However, due to the metallic NbS₂⁵⁵ or VS₂⁵⁶ layers, the MoS₂/NbS₂ and MoS₂/VS₂ heterostructures show metallic behavior, which will render significantly higher electrical conductivities than bulk 2H-MoS₂.

Thus, TMD heterostructures provide an opportunity to tailor the phase transformation behavior of the constituent layers and, at the same time, can result in improved battery performance in terms of capacitance and electrical conductivities. The insights gained from charge transfer calculations suggest that stable heterostructures can be designed by combing individual layers of phase transforming and non-phase transformation TMDs, such that the non-transforming phase exhibits stronger binding with incoming ions. The heterostructures are lighter than bulk MoS₂, which leads to significant improvement of the theoretical capacity. In addition to the gain in phase stability and capacities, the addition of metallic NbS₂ or VS₂ layers has been shown to decrease the electronic band gap of 2H-MoS₂, which can, in turn, result in better electrical conductivity. This study demonstrates a novel method for phase stabilization during ion cycling in batteries by the creation of vdW heterostructures. Similar studies on heterostructures of WS₂/NbS₂, WS₂/VS₂, etc., can be performed to validate this claim.

Conclusion

This paper investigates an approach to impede the phase transformation behavior of TMDs observed during ion intercalation. The approach is based on combining the phase-transforming TMDs with other TMDs that do not phase-transform during ion intercalation to create vdW heterostructures. The model phase-transforming TMD is chosen to be MoS₂ which transforms from 2H to 1T phase in the intercalation of Li-, Na-, and K-ions, whereas the non-transforming TMD is chosen to be VS₂ and NbS₂, which do not phase transformation during ion intercalation. The phase stability is investigated based on the total energies of the intercalated multilayered heterostructures for various configurations of the number of MoS₂ layers. The study explores the chemical origin of the phase transformation in MoS₂ by scrutinizing the charge transfer and binding characteristics. DFT simulations suggest that the presence of an NbS₂ layer impedes the intercalation-induced 2H→1T phase transformation in MoS₂ layers that are adjacent to the NbS₂ layer as well as up to the third-nearest neighbor layer from the NbS₂ layer for Na-ion and K-ion intercalation. However, the NbS₂ layer is unable to impede this phase transformation behavior for Li-ion intercalation, even for monolayer heterostructures. Similarly, the presence of a VS₂ layer impedes the MoS₂ phase transformation behavior during Li-ion, Na-ion, and K-ion intercalation. The ability to impede the phase transformation behavior of MoS₂ layers is dependent on the net negative charge rendered on the MoS₂ layer during ion intercalation. This study demonstrates that TMD heterostructures provide an opportunity to tailor the phase transformation behavior of the constituent layers and, at the same time, can result in improved battery performance in terms of capacitance and electrical conductivities. Such computational studies can also be useful in testing the viability of building heterostructures of other 2D materials, such as layered olivines, spinels, MXenes, etc.

Methods

Density functional theory. The first-principles calculations are carried out within the framework of density functional theory (DFT) using the Vienna Ab-initio Simulation Package (VASP)⁵⁷. The wave function is represented by a plane-wave basis with an energy cut-off of 500 eV. Ion-electron interactions are expressed by the projector augmented-wave (PAW)⁵⁸ method, and the generalized gradient approximation formulated by Perdew-Burke-Ernzerhof (GGA-PBE)⁵⁹ is used to express electronic exchange correlations. Periodic boundary conditions are applied so that the unit cell repeats in all directions. The structural parameters for the cell are

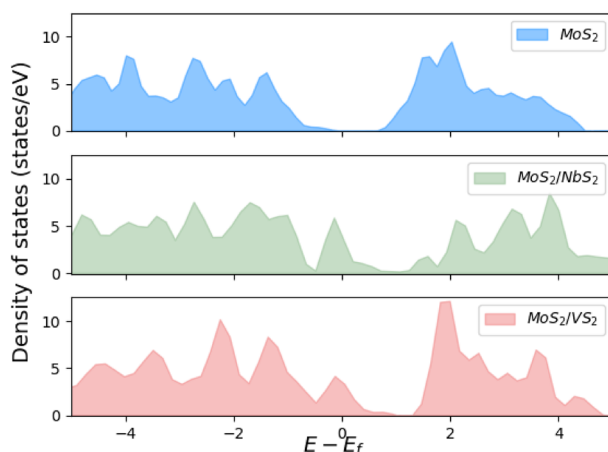


Figure 8. The density of states (DOSs) plots of 2H-MoS₂ (top), 2H-MoS₂/2H-NbS₂ (middle), and 2H-MoS₂/2H-VS₂ (bottom). Here, E_f denotes the energy of the Fermi level.

optimized using the conjugate gradient scheme, and the convergence threshold for residual forces on each atom is set to be 0.01 eV/Å. The DFT-D3 method of Grimme with Becke-Jonson damping⁶⁰ is used to model the vdW interaction between layers in MoS₂/NbS₂ systems as it represents well both the relative stability of phases and the structural parameters. DFT-D3 has been extensively used in the literature to model multilayer NbS₂ and other TMDs^{61–63}. For studying such effects in MoS₂/VS₂ heterostructures, the DFT-D3 method of Grimme with zero damping has been used to add vdW corrections. This method reproduced structural parameters and phase stabilities of different VS₂ phases well and has, thus, been also used in previous DFT studies⁶⁴.

Data availability

The datasets used and/or analysed during the current study available from the corresponding author on reasonable request.

Received: 28 November 2022; Accepted: 10 March 2023

Published online: 03 April 2023

References

- Sasaki, T., Ukyo, Y. & Novák, P. Memory effect in a lithium-ion battery. *Nat. Mater.* **12**, 569–575. <https://doi.org/10.1038/nmat3623> (2013).
- Yoshino, A. The birth of the lithium-ion battery. *Angew. Chem. Int. Ed.* **51**, 5798–5800. <https://doi.org/10.1002/anie.201105006> (2012).
- Scrosati, B. Recent advances in lithium ion battery materials. *Electrochim. Acta* **45**, 2461–2466. [https://doi.org/10.1016/S0013-4686\(00\)00333-9](https://doi.org/10.1016/S0013-4686(00)00333-9) (2000).
- Yi, T.-F. *et al.* A review of niobium oxides based nanocomposites for lithium-ion batteries, sodium-ion batteries and supercapacitors. *Nano Energy* **85**, 105955. <https://doi.org/10.1016/j.nanoen.2021.105955> (2021).
- Vincent, C. & Scrosati, B. *Modern Batteries* (Elsevier, 1997).
- Peng, L., Zhu, Y., Chen, D., Ruoff, R. S. & Yu, G. Two-dimensional materials for beyond-lithium-ion batteries. *Adv. Energy Mater.* **6**, 1600025. <https://doi.org/10.1002/aenm.201600025> (2016).
- Lv, X., Wei, W., Huang, B. & Dai, Y. Achieving high energy density for lithium-ion battery anodes by Si/C nanostructure design. *J. Mater. Chem. A* **7**, 2165–2171. <https://doi.org/10.1039/C8TA10936B> (2019).
- David, L., Bhandavat, R. & Singh, G. MoS₂/graphene composite paper for sodium-ion battery electrodes. *ACS Nano* **8**, 1759–1770. <https://doi.org/10.1021/nn406156b> (2014).
- Jiang, Y. *et al.* Transition metal oxides for high performance sodium ion battery anodes. *Nano Energy* **5**, 60–66. <https://doi.org/10.1016/j.nanoen.2014.02.002> (2014).
- Yu, A., Pan, Q., Zhang, M., Xie, D. & Tang, Y. Fast rate and long life potassium-ion based dual-ion battery through 3D porous organic negative electrode. *Adv. Funct. Mater.* **30**, 2001440. <https://doi.org/10.1002/adfm.202001440> (2020).
- Fedotov, S. S. *et al.* Titanium-based potassium-ion battery positive electrode with extraordinarily high redox potential. *Nat. Commun.* **11**, 1484. <https://doi.org/10.1038/s41467-020-15244-6> (2020).
- Liang, Y., Dong, H., Aurbach, D. & Yao, Y. Current status and future directions of multivalent metal-ion batteries. *Nat. Energy* **5**, 646–656. <https://doi.org/10.1038/s41560-020-0655-0> (2020).
- Niu, J., Zhang, Z. & Aurbach, D. Alloy anode materials for rechargeable Mg Ion batteries. *Adv. Energy Mater.* **10**, 2000697. <https://doi.org/10.1002/aenm.202000697> (2020).
- Blondeau, L., Surblé, S., Foy, E., Khodja, H. & Gauthier, M. Electrochemical reactivity of In-Pb solid solution as a negative electrode for rechargeable Mg-ion batteries. *J. Energy Chem.* **55**, 124–128. <https://doi.org/10.1016/j.jechem.2020.07.004> (2021).
- Tang, X. *et al.* A universal strategy towards high-energy aqueous multivalent-ion batteries. *Nat. Commun.* **12**, 2857. <https://doi.org/10.1038/s41467-021-23209-6> (2021).
- Hassanpour, A. *et al.* Magnesium and calcium ion batteries based on the hexa-peri-hexabenzocoronene nanographene anode materials. *Inorg. Chem. Commun.* **129**, 108656. <https://doi.org/10.1016/j.inoche.2021.108656> (2021).
- Wang, D. *et al.* A manganese hexacyanoferrate framework with enlarged ion tunnels and two-species redox reaction for aqueous Al-ion batteries. *Nano Energy* **84**, 105945. <https://doi.org/10.1016/j.nanoen.2021.105945> (2021).
- Feng, C. *et al.* Synthesis of molybdenum disulfide (MoS₂) for lithium ion battery applications. *Mater. Res. Bull.* **44**, 1811–1815. <https://doi.org/10.1016/j.materresbull.2009.05.018> (2009).
- Feng, C., Huang, L., Guo, Z. & Liu, H. Synthesis of tungsten disulfide (WS₂) nanoflakes for lithium ion battery application. *Electrochem. Commun.* **9**, 119–122. <https://doi.org/10.1016/j.elecom.2006.08.048> (2007).
- Zhou, P. *et al.* Colloidal WSe₂ nanocrystals as anodes for lithium-ion batteries. *Nanoscale* **12**, 22307–22316. <https://doi.org/10.1039/D0NR05691J> (2020).
- Chrissafis, K. *et al.* Structural studies of MoS₂ intercalated by lithium. *Mater. Sci. Eng. B* **3**, 145–151. [https://doi.org/10.1016/0921-5107\(89\)90194-3](https://doi.org/10.1016/0921-5107(89)90194-3) (1989).
- Parida, S. *et al.* Vertically stacked 2H–1T dual-phase MoS₂ microstructures during lithium intercalation: A first principles study. *J. Am. Ceram. Soc.* **103**, 6603–6614. <https://doi.org/10.1111/jace.17367> (2020).
- de Rezende Neto, A. S. & Seixas, L. Toward a two-dimensional NbS₂-based electrode for lithium-ion batteries. *Int. J. Quantum Chem.* **121**, e26603. <https://doi.org/10.1002/qua.26603> (2021).
- Samal, R. & Rout, C. S. Recent developments on emerging properties, growth approaches, and advanced applications of metallic 2D layered vanadium dichalcogenides. *Adv. Mater. Interfaces* **7**, 1901682. <https://doi.org/10.1002/admi.201901682> (2020).
- Zhang, G., Liu, H., Qu, J. & Li, J. Two-dimensional layered MoS₂: rational design, properties and electrochemical applications. *Energy Environ. Sci.* **9**, 1190–1209. <https://doi.org/10.1039/C5EE03761A> (2016).
- Liao, Y., Park, K.-S., Singh, P., Li, W. & Goodenough, J. B. Reinvestigation of the electrochemical lithium intercalation in 2H- and 3R-NbS₂. *J. Power Sources* **245**, 27–32. <https://doi.org/10.1016/j.jpowsour.2013.06.048> (2014).
- Stanje, B., Epp, V., Nakhil, S., Lerch, M. & Wilkening, M. Li ion dynamics along the inner surfaces of layer-structured 2H–Li_xNbS₂. *ACS Appl. Mater. Interfaces* **7**, 4089–4099. <https://doi.org/10.1021/am5078655> (2015).
- Janish, M. T. & Carter, C. B. In situ TEM observations of the lithiation of molybdenum disulfide. *Scr. Mater.* **107**, 22–25. <https://doi.org/10.1016/j.scriptamat.2015.05.011> (2015).
- Ghosh, C. *et al.* Characterizing Li in partially lithiated layer materials using atomic-resolution imaging, modeling, and simulation. *J. Am. Ceram. Soc.* **105**, 1581–1595. <https://doi.org/10.1111/jace.18189> (2022).
- Ghosh, C. *et al.* Phase evolution and structural modulation during in situ lithiation of MoS₂, WS₂ and graphite in TEM. *Sci. Rep.* **11**, 9014. <https://doi.org/10.1038/s41598-021-88395-1> (2021).
- Py, M. A. & Haering, R. R. Structural destabilization induced by lithium intercalation in MoS₂ and related compounds. *Can. J. Phys.* **61**, 76–84. <https://doi.org/10.1139/p83-013> (1983).

32. Wang, H. *et al.* Electrochemical tuning of vertically aligned MoS₂ nanofilms and its application in improving hydrogen evolution reaction. *Proc. Natl. Acad. Sci.* **110**, 19701. <https://doi.org/10.1073/pnas.1316792110> (2013).
33. Cook, J. B. *et al.* Suppression of electrochemically driven phase transitions in nanostructured MoS₂ pseudocapacitors probed using operando X-ray diffraction. *ACS Nano* **13**, 1223–1231. <https://doi.org/10.1021/acsnano.8b06381> (2019).
34. Van der Ven, A., Garikipati, K., Kim, S. & Wagemaker, M. The role of coherency strains on phase stability in Li_xFePO₄: Needle crystallites minimize coherency strain and overpotential. *J. Electrochem. Soc.* **156**, A949. <https://doi.org/10.1149/1.3222746> (2009).
35. Novoselov, K. S., Mishchenko, A., Carvalho, A. & Castro Neto, A. H. 2D materials and van der Waals heterostructures. *Science* **353**, aac9439. <https://doi.org/10.1126/science.aac9439> (2016).
36. Geim, A. K. & Van der Grigorieva, I. V. Waals heterostructures. *Nature* **499**, 419–425. <https://doi.org/10.1038/nature12385> (2013).
37. Zhang, M., Tang, C., Cheng, W. & Fu, L. The first-principles study on the performance of the graphene/WS₂ heterostructure as an anode material of Li-ion battery. *J. Alloys Compd.* **855**, 157432. <https://doi.org/10.1016/j.jallcom.2020.157432> (2021).
38. Wang, D., Liu, L.-M., Zhao, S.-J., Hu, Z.-Y. & Liu, H. Potential application of metal dichalcogenides double-layered heterostructures as anode materials for Li-ion batteries. *J. Phys. Chem. C* **120**, 4779–4788. <https://doi.org/10.1021/acs.jpcc.5b11677> (2016).
39. Fatima, N. *et al.* Influence of van der Waals heterostructures of 2D materials on catalytic performance of ZnO and its applications in energy: A review. *Int. J. Hydrog. Energy* **46**, 25413–25423. <https://doi.org/10.1016/j.ijhydene.2021.05.086> (2021).
40. Blackstone, C. & Ignaszak, A. Van der Waals heterostructures—Recent progress in electrode materials for clean energy applications. *Materials* <https://doi.org/10.3390/ma14133754> (2021).
41. Zhong, D. *et al.* Van der Waals engineering of ferromagnetic semiconductor heterostructures for spin and valleytronics. *Sci. Adv.* **3**, e1603113. <https://doi.org/10.1126/sciadv.1603113> (2017).
42. Xue, J. *et al.* Scanning tunnelling microscopy and spectroscopy of ultra-flat graphene on hexagonal boron nitride. *Nat. Mater.* **10**, 282–285. <https://doi.org/10.1038/nmat2968> (2011).
43. Peng, Q., Wang, Z., Sa, B., Wu, B. & Sun, Z. Blue phosphorene/MS₂ (M = Nb, Ta) heterostructures as promising flexible anodes for lithium-ion batteries. *ACS Appl. Mater. Interfaces* **8**, 13449–13457. <https://doi.org/10.1021/acsmi.6b03368> (2016).
44. Wang, J., Wang, B. & Lu, B. Nature of novel 2D van der Waals heterostructures for superior potassium ion batteries. *Adv. Energy Mater.* **10**, 2000884. <https://doi.org/10.1002/aenm.202000884> (2020).
45. Zhao, C. *et al.* Self-assembly-induced alternately stacked single-layer MoS₂ and N-doped graphene: A novel van der Waals heterostructure for lithium-ion batteries. *ACS Appl. Mater. Interfaces* **8**, 2372–2379. <https://doi.org/10.1021/acsmi.5b11492> (2016).
46. Fan, S. *et al.* Theoretical investigation of the intercalation chemistry of lithium/sodium ions in transition metal dichalcogenides. *J. Phys. Chem. C* **121**, 13599–13605. <https://doi.org/10.1021/acs.jpcc.7b05303> (2017).
47. Zhang, H., Liu, L.-M. & Lau, W.-M. Dimension-dependent phase transition and magnetic properties of VS₂. *J. Mater. Chem. A* **1**, 10821–10828. <https://doi.org/10.1039/C3TA12098H> (2013).
48. Zhang, X. *et al.* Insights into the storage mechanism of layered VS₂ cathode in Alkali metal-ion batteries. *Adv. Energy Mater.* **10**, 1904118. <https://doi.org/10.1002/aenm.201904118> (2020).
49. Yu, M. & Trinkle, D. R. Accurate and efficient algorithm for Bader charge integration. *J. Chem. Phys.* **134**, 064111. <https://doi.org/10.1063/1.3553716> (2011).
50. He, Q., Yu, B., Li, Z. & Zhao, Y. Density functional theory for battery materials. *Energy Environ. Sci.* **2**, 264–279. <https://doi.org/10.1002/eeem2.12056> (2019).
51. Stephenson, T., Li, Z., Olsen, B. & Mitlin, D. Lithium ion battery applications of molybdenum disulfide (MoS₂) nanocomposites. *Energy Environ. Sci.* **7**, 209–231. <https://doi.org/10.1039/C3EE42591F> (2014).
52. Gong, S., Zhao, G., Lyu, P. & Sun, K. Insights into the intrinsic capacity of interlayer-expanded MoS₂ as a Li-ion intercalation host. *J. Mater. Chem. A* **7**, 1187–1195. <https://doi.org/10.1039/C8TA08120D> (2019).
53. Rahman, I. A. & Purqon, A. First principles study of molybdenum disulfide electronic structure. *J. Phys. Conf. Ser.* **877**, 012026. <https://doi.org/10.1088/1742-6596/877/1/012026> (2017).
54. Peng, C. *et al.* Construction of 1T@2H MoS₂ heterostructures in situ from natural molybdenite with enhanced electrochemical performance for lithium-ion batteries. *RSC Adv.* **11**, 33481–33489. <https://doi.org/10.1039/D1RA05565H> (2021).
55. Zhao, S. *et al.* Two-dimensional metallic NbS₂: Growth, optical identification and transport properties. *2D Mater* **3**, 025027. <https://doi.org/10.1088/2053-1583/3/2/025027> (2016).
56. Wasey, A. H. M. A., Chakrabarty, S. & Das, G. P. Quantum size effects in layered VX₂ (X = S, Se) materials: Manifestation of metal to semimetal or semiconductor transition. *J. Appl. Phys.* **117**, 064313. <https://doi.org/10.1063/1.4908114> (2015).
57. Kresse, G. & Hafner, J. Ab initio molecular dynamics for liquid metals. *Phys. Rev. B* **47**, 558–561. <https://doi.org/10.1103/PhysRevB.47.558> (1993).
58. Blöchl, P. E. Projector augmented-wave method. *Phys. Rev. B* **50**, 17953–17979. <https://doi.org/10.1103/PhysRevB.50.17953> (1994).
59. Perdew, J. P., Burke, K. & Ernzerhof, M. Generalized gradient approximation made simple. *Phys. Rev. Lett.* **77**, 3865–3868. <https://doi.org/10.1103/PhysRevLett.77.3865> (1996).
60. Grimme, S., Ehrlich, S. & Goerigk, L. Effect of the damping function in dispersion corrected density functional theory. *J. Comput. Chem.* **32**, 1456–1465. <https://doi.org/10.1002/jcc.21759> (2011).
61. Ma, Y., Kuc, A., Jing, Y., Philipsen, P. & Heine, T. Two-dimensional haeckelite NbS₂: A diamagnetic high-mobility semiconductor with Nb⁴⁺ ions. *Angew. Chem. Int. Ed.* **56**, 10214–10218. <https://doi.org/10.1002/anie.201702450> (2017).
62. Golsanamlou, Z., Sementa, L., Cusati, T., Iannaccone, G. & Fortunelli, A. Theoretical analysis of a 2D metallic/semiconducting transition-metal dichalcogenide NbS₂/WSe₂ hybrid interface. *Adv. Theory Simul.* **3**, 2000164. <https://doi.org/10.1002/adts.202000164> (2020).
63. Zhao, S. *et al.* Group VB transition metal dichalcogenides for oxygen reduction reaction and strain-enhanced activity governed by p-orbital electrons of chalcogen. *Nano Res.* **12**, 925–930. <https://doi.org/10.1007/s12274-019-2326-7> (2019).
64. Wang, D. *et al.* Two-dimensional VS₂ monolayers as potential anode materials for lithium-ion batteries and beyond: first-principles calculations. *J. Mater. Chem. A* **5**, 21370–21377. <https://doi.org/10.1039/C7TA06944H> (2017).

Acknowledgements

The authors thank Drs Manish Singh and Chanchal Ghosh for their valuable inputs towards this work and acknowledge support from CINT through user proposals. CINT is the Center for Integrated Nanotechnology, which is a User Facility supported by the DOE at Sandia and Los Alamos National Laboratories. The authors would also like to acknowledge the High-Performance Computing (HPC) facilities at UConn and LANL for providing resources required to carry out this work.

Author contributions

The manuscript is written through the contributions of all authors. All authors have given approval for the final version of the manuscript.

Funding

This work is supported by the National Science Foundation (NSF) under Grant No. DMR-1820565.

Competing interests

The authors declare no competing interests.

Additional information

Supplementary Information The online version contains supplementary material available at <https://doi.org/10.1038/s41598-023-31342-z>.

Correspondence and requests for materials should be addressed to A.M.D.

Reprints and permissions information is available at www.nature.com/reprints.

Publisher's note Springer Nature remains neutral with regard to jurisdictional claims in published maps and institutional affiliations.



Open Access This article is licensed under a Creative Commons Attribution 4.0 International License, which permits use, sharing, adaptation, distribution and reproduction in any medium or format, as long as you give appropriate credit to the original author(s) and the source, provide a link to the Creative Commons licence, and indicate if changes were made. The images or other third party material in this article are included in the article's Creative Commons licence, unless indicated otherwise in a credit line to the material. If material is not included in the article's Creative Commons licence and your intended use is not permitted by statutory regulation or exceeds the permitted use, you will need to obtain permission directly from the copyright holder. To view a copy of this licence, visit <http://creativecommons.org/licenses/by/4.0/>.

© The Author(s) 2023